$Zr_4O_5N_2$ − Intergrowth of Fluorite and Bixbyite Anion Layers Formed by Coupled Site-Selective Anion and Vacancy Ordering

C. W. Michie,† J. B. Claridge,† S. J. Clarke,*,‡ and M. J. Rosseinsky*,†

Department of Chemistry, The University of Liverpool, Liverpool L69 7ZD, U.K., and Inorganic Chemistry Laboratory, Department of Chemistry, University of Oxford, South Parks Road, Oxford OX1 3QR, U.K.

Received January 2, 2003

The defect fluorite $Zr_4O_5N_2$ is presented. A simple layered intergrowth of the important bixbyite and fluorite structure types, it displays an A_4X_7 vacancy ordering alternative to that in the pyrochlore and other structures. This ordering is stabilized by proximity of the highly charged N^{3-} anions to the bixbyite-type face diagonal vacancy neighbors in the initially cubic cation coordination environment of fluorite. The existence of this simple structure demonstrates the potential of substitution on the anion sublattice to control the structures of ionic defect systems.

Introduction

The fluorite structure is one of the most important binary types. Controlled introduction of vacancies on the anion sublattice produces oxide anion mobility that is exploited in solid electrolyte behavior in gas sensors[1] and fuel cells[2] in materials such as the cubic stabilized zirconias. The detailed behavior of oxide anion vacancies in cubic stabilized fluorites is thus of considerable and growing technological importance. Complex vacancy ordering patterns in these phases have been intensively studied for their crystallographic significance[3] but are of direct relevance to the transport properties of long-range disordered fluorites as the motifs may control short-range ordering or clustering of vacancies and thus transport behavior.[4] Recent studies reveal that even systems that are cubic as judged by the metric symmetry derived from Bragg scattering can display complex modulated structures suggestive of a variety of short-range ordered local cation environments.[5] Incommensurately or commensurately compositionally and displacively modulated derivatives of fluorites can be built up from these structural principles.[6] The $A_2B_2O_7$ pyrochlore[7] and A_2O_3 bixbyite[8] structures are particularly significant vacancy-ordered derivatives of fluorite which are common in the structural chemistry of the oxides of the transition metal, lanthanide, and actinide elements. Figure 1 shows modular representations of the pyrochlore and bixbyite structures, with the anion vacancies within each fluorite subcell in the unit cells shown as gray tetrahedra of metal sites surrounding the vacancy. Anion vacancy stabilization in oxides is generally driven by the composition and resulting charge of the cation sublattice. However, it is possible to generate

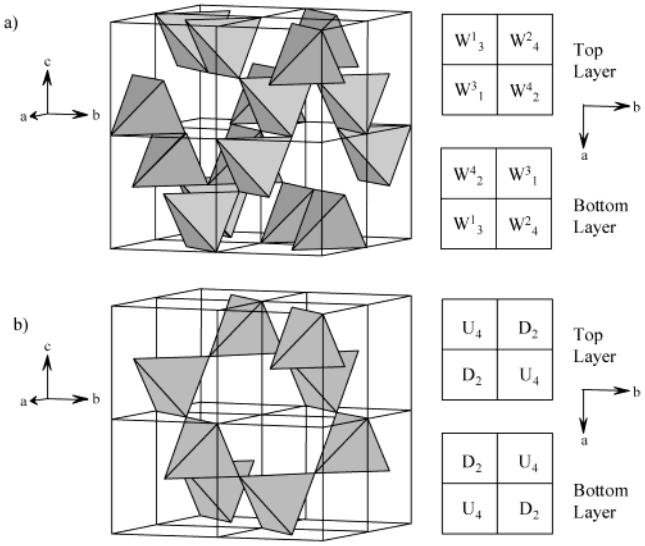

Figure 1. Modular representation of the A_2X_3 bixbyite (a) and A_4X_7 pyrochlore (b) structures. The anion vacancies are shown as gray A_4 tetrahedra located in each of the eight fluorite subcells into which the cell has been divided. To the right is shown the modular stacking sequence of the top and the bottom layers, in which the orientation of the $A_4\square$ tetrahedron is specified according to ref 14.[14] D indicates a fluorite module with an anion vacancy in the bottom part of the cell, U indicates one in which the vacancy is in the top part, and W represents one with vacancies in both top and bottom. The subscripts and superscripts indicate the quadrant of the module in which the vacancy is located.

* To whom correspondence should be addressed. Phone: 44-151-794-3499. Fax: 44-151-794-3588. E-mail: m.j.rosseinsky@liv.ac.uk; simon.clarke@chem.ox.ac.uk.
† The University of Liverpool.
‡ University of Oxford.

(1) Benammar, M. *Meas. Sci. Technol.* **1994**, *5*, 757−767.
(2) Minh, N. Q. *J. Am. Ceram. Soc.* **1993**, *76*, 563−588.
(3) Tabira, Y.; Withers, R. L.; Barry, J. C.; Elcoro, L. *J. Solid State Chem.* **2001**, *159*, 121−129.
(4) Goff, J. P.; Hayes, W.; Hull, S.; Hutchings, M. T.; Clausen, K. N. *Phys. Rev. B* **1999**, *59*, 14202−14219.
(5) Ling, C. D.; Withers, R. L.; Schmid, S.; Thompson, J. G. *J. Solid State Chem.* **1998**, *137*, 42−61.
(6) Welberry, T. R.; Withers, R. L.; Mayo, S. C. *J. Solid State Chem.* **1995**, *115*, 43−54.
(7) Subramanian, M. A.; Aravamudan, G.; Rao, G. V. S. *Prog. Solid State Chem.* **1983**, *15*, 55−141.
(8) Pauling, L.; Shappell, M. A. *Z. Kristallogr.* **1930**, *A75*, 128−142.

10.1021/cm0300415 CCC: $25.00
Published on Web 03/15/2003

such structures by aliovalent substitution of nitride on the oxide sublattice in the zirconium oxynitride family.[9−11] As both anion/vacancy ordering and ordering of different anions can affect the cation environment, this family of defect fluorites offers, in principle, a route to new vacancy-ordered structures. The A_4X_7 composition of pyrochlore requires one anion vacancy for every fluorite unit cell of dimension a_F, and derives from the long range order of these vacancies in an 8-fold ($2a_F \times 2a_F \times 2a_F$) supercell.

In this paper we present the A_4X_7-phase $Zr_4O_5N_2$ in which the anion vacancies order to form a new structure type constructed by strict alternation of fluorite and bixbyite anion layers, with an ordered array of six-, seven-, and eight-coordinate sites occupied by the same cation. Its formation appears to be driven by strong coupling between ordering of anions and vacancies and of the oxide and nitride species on the occupied anion sites. This demonstrates that anion substitution to form mixed anion phases can generate structures not readily isolable by manipulation of the cation alone. The existence of differing cation coordination environments with coupling between coordination number and anion type suggests rich potential for substitutional chemistry. Materials with layered structural motifs are of considerable interest, and this new fluorite derivative is thus a significant addition to the array of characterized ternary structures.

Experimental Section

Synthesis. Materials of composition $Zr_4O_5N_2$ were prepared on a 0.5- to 2-g scale by reaction of Zr_2ON_2 (prepared by ammonolysis of ZrO_2 as in reference 10) with monoclinic ZrO_2 (low hafnia grade, 99.99%, Aldrich Chemical Co.) in silica ampules (sealed under a vacuum of at least 1×10^{-1} Torr) at 720−760 °C until the reaction was complete, as judged by the absence of further changes in the X-ray powder diffraction pattern. The sample (approximately 0.45 g) characterized by synchrotron X-ray diffraction was prepared at 720 °C for 2 × 5 days with an intermediate regrinding. The sample (approximately 2 g) characterized by neutron diffraction was prepared at 750 °C for 2 × 40 h, followed by 40 h and finally 65 h at 760 °C, with intermediate regrinding. The N content was analyzed by CHN analysis using a Carlo Erber Strumentazione 1106 CHN analyzer. The samples characterized by synchrotron X-ray and neutron diffraction had N contents of 5.9(2)% (the expected value for $Zr_4O_5N_2$ is 5.92%). Reoxidation of the neutron diffraction sample under O_2 on a gravimetric balance showed a mass increase of 4.2(2) % (the expected mass increase for the reoxidation of $Zr_4O_5N_2$ is 4.22%).

Structural Characterization. The progress of synthetic reactions was monitored using a Stoe Stadi−P diffractometer in thin film transmission geometry with Cu $K\alpha_1$ radiation and a position-sensitive detector. Synchrotron powder X-ray diffraction data were collected in Hart−Parrish flat plate geometry at station 2.3 at the Synchrotron Radiation Source, Daresbury Laboratory ($\lambda = 1.3997$ Å) over $14.01 \leq 2\theta/° \leq 115.96$ with a step size of 0.01° and a counting time of 2.5 s per step. Rietveld analysis was performed with the GSAS suite, with a pseudo-Voigt peakshape function and an eight-term shifted Chebyschev function to model the background. Powder neutron diffraction data were collected on 1.4 g of sample sealed in a thin-walled evacuated 10-mm-diameter spectrosil ampule placed in a 12-mm-diameter vanadium can. Data were collected on the high-resolution powder diffractometer (HRPD) at the ISIS spallation neutron source for 97.2 μAhours and the structure was refined against data from the backscattering detector bank ($2\theta = 165°$). The peakshape was modeled as a convolution of back-to-back exponentials with a pseudo-Voigt function, and the background was modeled using an eight-term shifted Chebyschev function.

Results

The diffraction pattern of $Zr_4O_5N_2$ is similar at low angle to that of the bixbyite Zr_2ON_2 but with a few additional weak reflections, and displays significant peak splitting at higher angle (Figure S1 in the Supporting Information). Autoindexing with the TREOR software[12] of the first 40 reflections of the laboratory powder X-ray diffraction pattern of $Zr_4O_5N_2$ yielded a tetragonal unit cell with $a = 10.1727(5)$ Å and $c = 10.1313(5)$ Å. Attempts to solve the structure by ab initio or maximum entropy methods failed, presumably due to the high level of pseudosymmetry in the structure. A structural model was therefore derived by setting up a trial structure in the lowest symmetry tetragonal space group $I4$ derived by $2a_F \times 2a_F \times 2a_F$ expansion of an $Fm\bar{3}m$ fluorite cell in which there are six cation and eight anion sites. The eight possible anion sites in the supercell are all on 8*c* general positions and the A_4X_7 composition requires that one of these sites must be vacant. The Zr positions were initially refined in $I4$ against the synchrotron data followed by the anion positions. This model was then refined against the neutron data with the anion positions represented as a compositionally disordered mixture of oxide and nitride. The positional and fractional occupancy parameters of the anion sites were refined with heavy (90%) damping. This refinement did not converge but the occupancy of the $^1/_8,^3/_8,^1/_8$ anion site had decreased significantly and its position had become significantly displaced from the ideal fluorite position. This indicated that the ($^1/_8,^3/_8,^1/_8$) position was the vacant site in the supercell. Inspection of the type I super groups of $I4$ reveals $I4mm$, $I4/m$, $I422$, $I4cm$, $I4/mmm$, and $I4/mcm$ as candidates. Only in $I4cm$ does the $^1/_8,^3/_8,^1/_8$ vacancy occupy an 8-fold site. Refinement of the synchrotron powder X-ray data proceeded smoothly in this space group, with application of a surface roughness absorption correction allowing refinement of distinct displacement parameters for the Zr sites. The resulting fit is shown in Figure 2(a) (agreement indices are shown in the caption), and the structural and positional parameters are given in Table 1 (which also contains parameters from refinement of the neutron diffraction data). The high resolution and statistical quality of the synchrotron data allow stable refinement of the anion positions with chemically sensible bond lengths.

Refinement against powder neutron diffraction data is required to investigate possible oxide/nitride ordering due to the differing scattering lengths (O, 5.81 fm; N, 9.36 fm). Refinement with a statistical anion distribution proceeded smoothly to $\chi^2 = 2.55$ with anion positions similar to those found in the synchrotron refine-

(9) Gilles, J. C. *Bull. Soc. Chim. Fr.* **1962**, *22*, 2118−2122.
(10) Clarke, S. J.; Michie, C. W.; Rosseinsky, M. J. *J. Solid State Chem.* **1999**, *146*, 399−405.
(11) Lerch, M. *J. Mater. Sci. Lett.* **1998**, *17*, 441−443.
(12) Werner, P.-E.; Eriksson, L.; Westdahl, M. *J. Appl. Crystallogr.* **1985**, *18*, 367−370.
(13) Howard, C. J.; Hill, R. J.; Reichert, B. E. *Acta Crystallogr.* **1988**, *B44*, 116.

Table 1. Positional Parameters and Temperature Factors from the Rietveld Refinements of $Zr_4O_5N_2$ against HPRD PND Data and Synchrotron PXRD Data[a]

	x	*y*	*z*	U_i/Å^2	Wyckoff position	fractional occupancy
Zr(1)	0	0	0	0.0079(3)†	4a	1
				0.0070(7)		
Zr(2)	1/2	0	0.9615(7)	0.0079(3)†	4b	1
			0.9600(3)	*0.0070(8)*		
Zr(3)	0.2303(4)	0.7303(4)	0.9763(8)	0.0079(3)†	8c	1
	0.2299(2)	*0.7299(2)*	*0.9776(5)*	*0.0071(8)*		
Zr(4)	0.2419(3)	0.0251(3)	0.2436(6)	0.0079(3)†	16d	1
	0.2414(2)	*0.0253(1)*	*0.2428(4)*	*0.0058(5)*		
O/N(1)	0.3903(3)	0.1097(3)	0.1075(8)	0.0076(3)*	8c	0.19(2):0.81(2)
	0.392(2)	*0.108(2)*	*0.104(3)*	*0.0139(8)*‡		
O/N(2)	0.3647(3)	0.1353(3)	0.3848(8)	0.0076(3)*	8c	0.45(3):0.55(3)
	0.361(1)	*0.139(1)*	*0.389(2)*	*0.0139(8)*‡		
O/N(3)	0.1167(4)	0.3833(4)	0.3190(8)	0.0076(3)*	8c	1:0
	0.118(1)	*0.382(1)*	*0.327(2)*	*0.0139(8)*‡		
O/N(4)	0.1173(4)	0.1521(3)	0.1165(7)	0.0076(3)*	16d	0.65(2):0.35(2)
	0.118(2)	*0.153(1)*	0.117(2)	*0.0139(8)*‡		
O/N(5)	0.3650(4)	0.3938(4)	0.3689(7)	0.0076(3)*	16d	1:0
	0.365(1)	*0.390(1)*	*0.369(2)*	*0.0139(8)*‡		
Vacancy	1/8	3/8	1/8	-	8c	-

[a] Values for the synchrotron PXRD refinement are shown in italics under the HPRD PND values.†,*,‡Refined as single parameters.

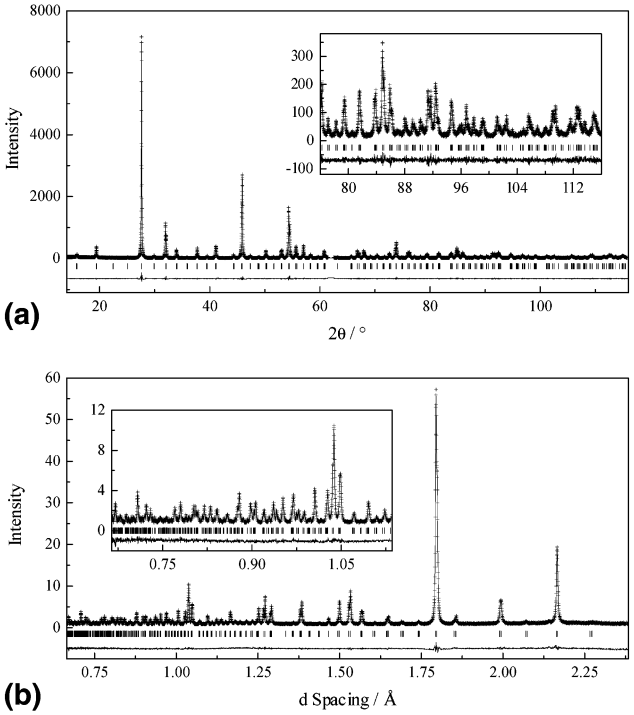

Figure 2. (a) Plot of Rietveld refinement of $Zr_4O_5N_2$ against synchrotron PXRD data (Daresbury 2.3, $\lambda = 1.3997$ Å).The observed points are shown as crosses, the calculated points are shown as a solid line, and the difference is shown as a solid line below. The tick marks indicate the position of Bragg reflections of $Zr_4O_5N_2$. $R_{wp} = 9.52\%$, $\chi^2 = 1.80$, $R(F^2) = 3.17\%$. (b) Plot of Rietveld refinement of $Zr_4O_5N_2$ against HRPD PND data. The observed points are shown as crosses, the calculated points are shown as a solid line, and the difference is shown as a solid line below. The tick marks indicate the position of Bragg reflections of $Zr_4O_5N_2$. $R_{wp} = 6.67\%$, $\chi^2 = 1.99$, $R(F^2) = 8.39\%$.

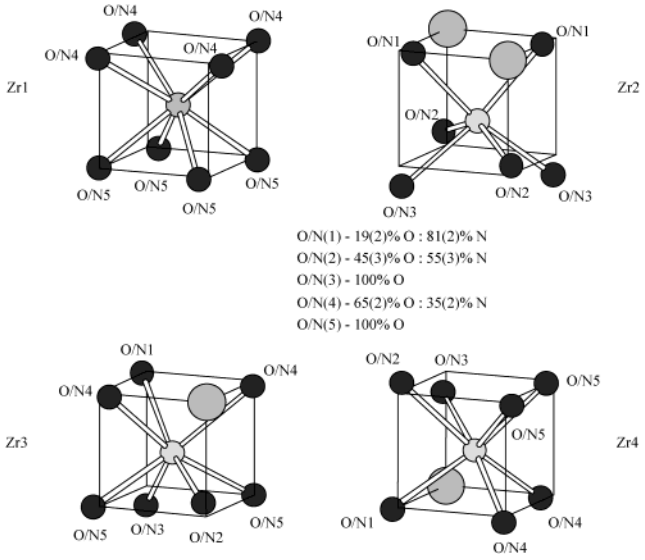

Figure 3. Coordination around the four symmetry-inequivalent zirconium sites in $Zr_4O_5N_2$. The anions are represented by the small dark gray spheres, the zirconiums are shown by the small light gray spheres, and the anion vacancies are represented by the large gray spheres. The cubes were formed by connecting the ideal fluorite anion positions.

ment. The observation of the *600* reflection violates the $I4_1$__ and I__d diffraction symbols, with the remaining absences being consistent with I_c_. LeBail extraction in *I*4/*mcm* gave agreement indices equivalent to those found in *I*4/*mmm*. All these observations confirm the assignment of the *I*4*cm* space group. Free refinement of the site compositions with each site constrained to be fully occupied reduced χ^2 to 1.98 but produced a refined composition of $Zr_4O_{4.48(9)}N_{2.52(9)}$. As this differs by more than 3σ from the composition determined by chemical analysis, the two most oxide-rich sites from the refinement were set as oxide only, and the anion ratios on the other two sites were refined to give a composition of $Zr_4O_{4.93(5)}N_{2.07(5)}$ and $\chi^2 = 1.99$. This is significantly improved over the disordered model but does require the chemical assumption outlined above. The resulting fit is shown in Figure 2(b), with the parameters given in Table 1.

The resulting structure has four inequivalent cation sites (Figure 3). Zr(1) is a cubic eight-coordinate site, Zr(2) is octahedral, and Zr(3) and Zr(4) are both seven-coordinate. Bond lengths from both refinements are given in Table 2, and bond angles from the HRPD refinement are given in Table S2 in the Supporting Information. The cubic Zr(1) site is coordinated by an

Table 2. Selected Bond Distances (in Å) from the Rietveld Refinements of $Zr_4O_5N_2$ against HPRD PND Data and Synchrotron PXRD Data

	HRPD (sample *A*)		Synchrotron (sample *C*)	
bond	distance(Å)	mean	distance(Å)	mean
Zr1−O/N4	2.282(5) × 4	2.24(4)	2.30(2) × 4	2.25(4)
Zr1−O/N5	2.195(5) × 4		2.21(2) × 4	
Zr2−O/N1	2.162(6) × 2	2.16(5)	2.13(2) × 2	2.14(2)
Zr2−O/N2	2.095(5) × 2		2.13(2) × 2	
Zr2−O/N3	2.214(7) × 2		2.17(2) × 2	
Zr3−O/N1	2.185(5)	2.20(5)	2.17(3)	2.18(5)
Zr3−O/N2	2.145(5)		2.09(2)	
Zr3−O/N3	2.282(5)		2.22(2)	
Zr3−O/N4	2.248(5) × 2		2.24(2) × 2	
Zr3−O/N5	2.157(5) × 2		2.14(2) × 2	
Zr4−O/N1	2.218(4)	2.18(3)	2.24(2)	2.20(4)
Zr4−O/N2	2.205(4)		2.24(2)	
Zr4−O/N3	2.175(4)		2.21(1)	
Zr4−O/N4	2.221(5)		2.21(2)	
Zr4−O/N4	2.142(5)		2.13(2)	
Zr4−O/N5	2.139(5)		2.17(2)	
Zr4−O/N5	2.183(5)		2.16(1)	
O/N1−Zr2	2.162(6)	2.20(2)	2.13(2)	2.20(5)
O/N1−Zr3	2.185(8)		2.17(3)	
O/N1−Zr4	2.218(4) × 2		2.24(2) × 2	
O/N2−Zr2	2.095(5)	2.16(5)	2.13(2)	2.17(7)
O/N2−Zr3	2.145(7)		2.09(2)	
O/N2−Zr4	2.205(4) × 2		2.24(2) × 2	
O/N3−Zr2	2.214(7)	2.21(4)	2.17(2)	2.20(2)
O/N3−Zr3	2.282(8)		2.22(2)	
O/N3−Zr4	2.175(4) × 2		2.21(1) × 2	
O/N4−Zr1	2.282(2)	2.22(5)	2.30(2)	2.22(6)
O/N4−Zr3	2.248(2)		2.24(2)	
O/N4−Zr4	2.221(2)		2.21(2)	
O/N4−Zr4	2.142(2)		2.13(2)	
O/N5−Zr1	2.195(2)	2.17(2)	2.21(2)	2.17(2)
O/N5−Zr3	2.157(2)		2.14(2)	
O/N5−Zr4	2.139(2)		2.17(2)	
O/N5−Zr4	2.183(1)		2.16(1)	
Vac−Zr2	2.444(5)	2.44(8)	2.455(2)	2.44(8)
Vac−Zr3	2.569(6)		2.566(4)	
Vac−Zr4	2.368(4) × 2		2.368(3) × 2	

anion site which is 100% oxide (O(5) is one face of the cube) and one which is 65% oxide (O/N(4)). The six-coordinate Zr(2) site has the divacancy required to generate octahedral coordination in the "bixbyite" rather than "pyrochlore" geometry with two cube corners separated by a face diagonal, rather than a body diagonal, being vacant. The remaining two sites on this face, immediately neighboring the vacancies, are occupied by the anion site O/N(1) which is the most (81(2)%) nitride rich. This lowest coordination number cation site has the highest level of nitride in its first coordination sphere (45%), utilizing the enhanced charge and coordinating power of the nitride anion to compensate for the anion vacancies. The mean bond lengths at the cation sites scale with the coordination number as expected, and the cation sites all relax away from the vacancy toward the occupied anion positions as is ubiquitous in these defect fluorite structures. The mean Zr−O/N bond lengths in this compound and other zirconium oxides and oxynitrides scale with the proportion of oxide and nitride neighbors, although it should be noted that the calculated mean Zr−O/N distances reported here have a large standard deviation from their mean values due to the departures of the sites from regular geometry. The cubic site in cubic zirconia has neighbors at 2.224 Å, slightly closer than the mean of 2.24(4) Å for the Zr(1) site in $Zr_4O_5N_2$ in which 17% of the coordinating anions are the more highly charged nitride ion. Similarly, the two seven-coordinate sites in $Zr_4O_5N_2$, both with 29% nitride in their coordination sphere and three oxide-only sites on the fully coordinated face of the cube, are coordinated by anions slightly more distant (Zr(3), 2.20(5) Å; Zr(4), 2.18(3) Å) than the oxide ions in baddeleyite ZrO_2 (2.159 Å).[13]

The octahedral Zr(2) site with anions on average 2.16(5) Å distant should be compared with the two octahedral sites in Zr_2ON_2 which have a higher concentration (66%) of nitride in their coordination sphere and correspondingly slightly longer Zr−O/N distances of 2.185(1) Å. The cubic Zr(1) site is distorted relative to the site in cubic zirconia on account of the two different sets of bond lengths to the O/N(4) and O/N(5) sites, and the Zr(2) site is in a highly distorted octahedral environment with bond angles similar to those for the 24*d* site in Zr_2ON_2. The bond angles around the Zr(3) and Zr(4) sites are comparable to those for the zirconium site in baddeleyite ZrO_2.

Discussion

The vacancy ordering in $A_2B_2O_7\square$ (A_4X_7) pyrochlore and $A_4O_6\square_2$ bixbyite is best discussed by considering the location of the vacancies in the original cubic coordination environment of the cation in the fluorite subcell. In the pyrochlore structure, ordered removal of two anions along a body diagonal of the cubic environment of half of the metal cations produces, after considerable relaxation of the remaining anions, a three-dimensional network of corner-sharing octahedra and accompanying zigzag chains of anion vacancies along ⟨110⟩ directions (Figure 1(b)). (This transformation may be formally described as proceeding from the $Fm\bar{3}m$ 5 Å $a_F \times a_F \times a_F$ fluorite cell via the $Pn\bar{3}m$ subgroup to a $2a_F \times 2a_F \times 2a_F$ $Fd\bar{3}m$ cell in which the 8*a* sites are vacant). The introduction of vacancies in this manner produces two distinct cation environments with octahedral (B sites) and cubic (A sites) geometry.

In the bixbyite Mn_2O_3 or C-type rare earth oxide structure there are twice as many anion vacancies as in pyrochlore. This reduces the coordination number of all the cations in the structure to six, with two distinct cation sites. The 8*a* sites are formed by the introduction of body diagonal vacancy pairs as in the pyrochlore structure but the six coordination at the remaining 24*d* sites is generated by the formation of vacancies at cube corners separated by face rather than body diagonals (Figure 1(a)). This results in the formation of a body-centered array of vacancies on the 16*c* $^1/_8,^1/_8,^1/_8$ positions of the $Ia\bar{3}$ space group. In this case the formal subgroup relationships pass from 5 Å $a_F \times a_F \times a_F$ $Fm\bar{3}m$ via $a_F \times a_F \times a_F$ $Pm\bar{3}m$ to $2a_F \times 2a_F \times 2a_F$ $Ia\bar{3}$. This $^1/_2\langle 110\rangle_F$ vacancy pair in bixbyite violates the vacancy ordering rules found in the R_nO_{2n-2m} ($n \geq 7$) rare earth oxide family[14] whose structures can be systematized based on fluorite subcell modules containing at most two anion vacancies separated by half the subcell body diagonal ($^1/_2\langle 111\rangle_F$).

The presence of a body-centered vacancy array in the $Zr_4O_5N_2$ structure suggests a structural analogy with bixbyite. The A_4X_7 composition then requires filling of half the vacant anion sites in bixbyite, leaving a body-

(14) Kang, Z. C.; Eyring, L. *J. Alloys Compd.* **1998**, *275−277*, 30−36.

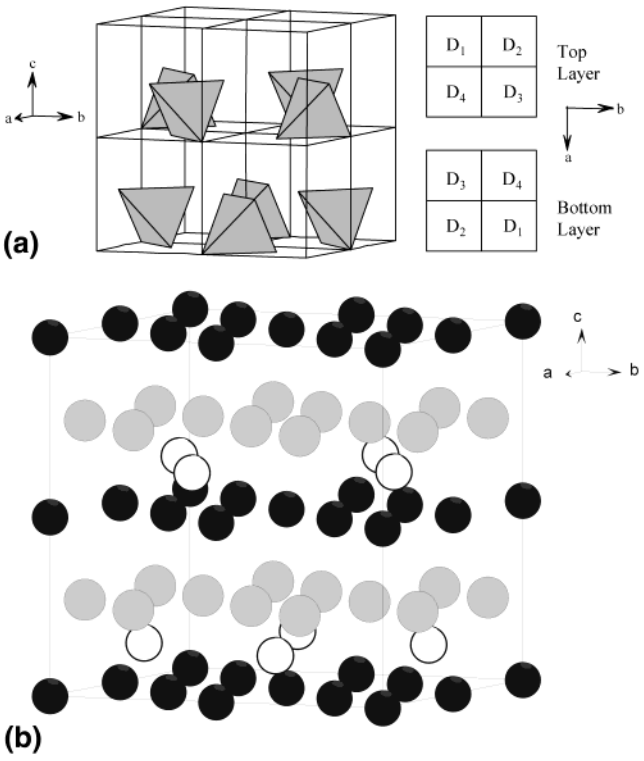

Figure 4. (a) Modular representation of the $Zr_4O_5N_2$ structure. The anion vacancies are shown as gray Zr_4 tetrahedra located in each of the eight fluorite subcells into which the cell has been divided. To the right is shown the modular stacking sequence of the top and the bottom layers, in which the orientation of the $Zr_4\square$ tetrahedron is specified according to ref 14.[14] The anion vacancies occur in alternate layers along the *c* stacking direction. Arrows indicate the intervening fully occupied layers of anion sites. Comparison with the bixbyite structure indicates that this structure is a layered intergrowth of bixbyite and fluorite. (b) Presence of vacancies (white spheres) in alternate anion layers produces layering of the cation sites: the seven-coordinate Zr(4) sites (grey) alternate with layers containing the six-, seven-, and eight-coordinate sites (black spheres).

centered relationship between the remaining vacant sites. Depiction of the structure using the tetrahedral cation group surrounding it to describe the vacancy (this $M_4\square$ unit, plus relaxation of the six oxides neighboring the vacancy, is commonly used in discussing fluorite-derived structures[15]) indicates a layered ordering scheme. (Figure 4(a)) There are four anion layers along the *c*-axis of the supercell (which consists of eight fluorite module subcells, each one containing a single vacancy) and the vacancies occur in half of these layers in a manner which strictly alternates along *c* (Figure 4(b)). The vacancy distribution within a layer precisely matches that found in bixbyite, with $^1/_2\langle 110\rangle_F$ (5.7 Å) closest intervacancy contacts. Inspection of the vacant anion site coordinates in the defect-containing layers in $Zr_4O_5N_2$ and bixbyite (Figure 5) reveals that they can be superposed with an origin shift of the bixbyite cell by $0.25 \times b$. The orientational and positional relationship between the anion vacancy-centered tetrahedra in alternate layers of bixbyite is identical to that in the successive

(15) Hoskins, B. F.; Martin, R. L. *J. Chem. Soc., Dalton Trans.* **1975**, *1*, 576.

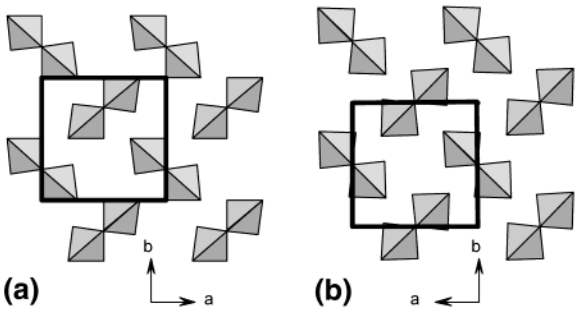

Figure 5. (a) Array of anion vacancies within a bixbyite layer of thickness of $^1/_2\ a_F$ in the cubic bixbyite Zr_2ON_2 structure.[10] The shaded tetrahedra represent Zr_4 vacancy units. (b) Extended layer of thickness of $^1/_2\ a_F$ of anion vacancies in $Zr_4O_5N_2$. The black squares are the crystallographic unit cells.

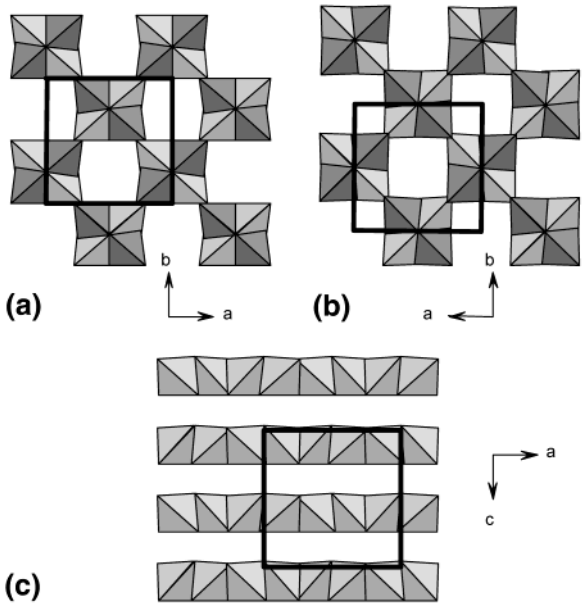

Figure 6. (a) View along the stacking direction of alternate layers of bixbyite vacancies in Zr_2ON_2,[10] represented as tetrahedra. (b) View along *c* of two sequential vacancy layers in the $Zr_4O_5N_2$ structure. The black squares are the crystallographic unit cells. In both cases the layers are $^1/_2\ a_F$ thick and the darker layer is a_F above the lighter layer. (c) $Zr_4O_5N_2$ viewed perpendicular to the layer stacking direction showing the bixbyite−fluorite intergrowth.

defect layers of $Zr_4O_5N_2$ (Figure 6). The structure is thus a layered intergrowth of alternating fluorite and bixbyite anion layers. The fluorite layers consist of the oxide-only O(3) and O(5) anion sites together with the 45% oxide O/N(2), while the bixbyite layers contain no oxide-only sites. The layering of the anions also gives layering of the cation sites, with seven-coordinate Zr(3) layers alternating with layers containing the six-, seven-, and eight-coordinate sites.

The locations of the octahedral Zr(2) sites in the layered $Zr_4O_5N_2$ phase can also be derived from the bixbyite set. They are arranged in columns along *c* with 5.1 Å separations between the centers of the octahedra and 7.2 Å separation between the columns. This can be achieved in bixbyite by selecting those octahedral positions which have two anion vacancies within the same layer as neighbors, thus producing a subset of the "face diagonal" 24*d* cation positions (Figure 7). The layered arrangement of the vacancies prevents the alternative "body diagonal" vacancy pair mechanism of forma-

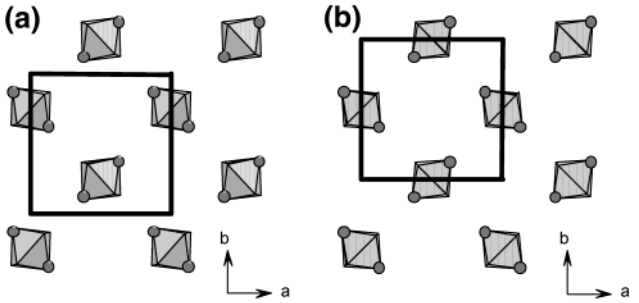

Figure 7. (a) Octahedral cation sites formed by anion vacancy pairs in face diagonal positions in a single bixbyite vacancy layer of thickness of $^1/_2$ a_F in Zr_2ON_2.[10] (b) Arrangement of octahedral columns in $Zr_4O_5N_2$ adopts the same pattern as that shown in (a). The anion vacancies are shown as gray spheres and the $Zr(O,N)_6$ units are shown as gray octahedra. If the vacancies were included in the coordination polyhedra, distorted cubes would be formed.

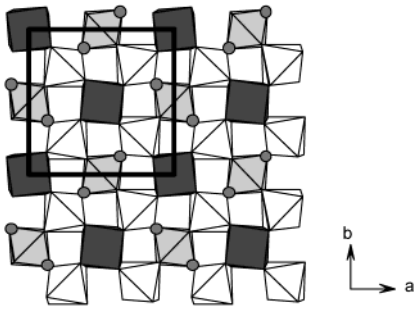

Figure 8. Interrelationship of the different cation polyhedra in $Zr_4O_5N_2$ in a layer of thickness of $^1/_2$ a_F. Zr(1) cubic site is dark gray, Zr(2) octahedral site is light gray, and Zr(3) seven-coordinate site is white. Above and below this layer there are seven-coordinate Zr(4) sites.

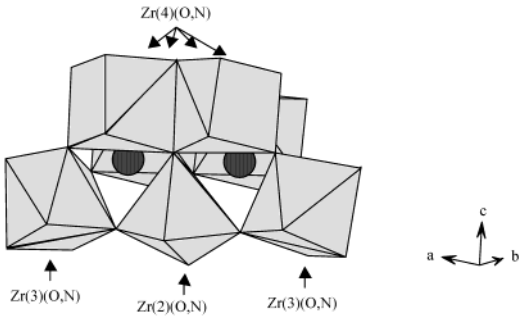

Figure 9. Octahedrally coordinated Zr(2) site has the two seven-coordinate sites in the structure as its near neighbors. Six of the twelve nearest neighbors are shown here.

tion of the octahedral sites, as this requires vacancies in neighboring anion layers. The purely cubic sites (Figure 8) also form columns parallel to *c*, connected to the octahedral Zr(2) columns by corner sharing with the columns of seven-coordinate Zr(3) sites and edge sharing with the columns of Zr(4) sites. The arrangement of the twelve neighbors of an octahedral Zr(2) site is depicted in Figure 9.

The layered vacancy ordering with the $^1/_2\langle 110\rangle_F$ vacancy pairs, usually disfavored for electrostatic reasons at this relatively low vacancy concentration, appears strongly coupled structurally to anion ordering. The nitride-rich O/N(1) sites are found in the layers containing the vacancies, bridging pairs of vacancies in forming parallelograms of vacant and nitride-rich sites, linked by vacancy-nitride contacts (Figure 10). The

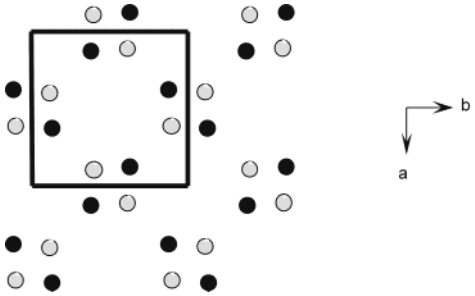

Figure 10. Vacancies (dark gray spheres) and nitride rich O/N(1) sites (light gray spheres) are nearest neighbors in the vacancy-containing layers of $Zr_4O_5N_2$.

nitride anions electrostatically stabilize the vacancies, and also provide enhanced covalent bonding at the octahedral Zr(2) site which has the two vacancies in its first coordination sphere. Within a single fluorite cube, the face-diagonal relationship of the vacancies creates two equivalent anion sites as nearest neighbors; because these sites differ from the remaining four sites on the opposite face of the cube, they can be preferentially occupied by site-selective anion ordering in a mixed anion solid. By contrast, a body-diagonal relationship of vacancy pairs creates six equivalent remaining sites, better suited by electrostatics in a monoanionic solid but impossible to optimize by anion site ordering in a multianion phase.

The defect-free and bixbyite-type layers in $Zr_4O_5N_2$ are separated because this nitride-stabilized $\langle 110\rangle_F$ vacancy order within a single fluorite subcell propagates in a layered manner throughout the rest of the structure. In pyrochlore and bixbyite the occurrence of body-diagonal vacancy pairs necessitates the existence of neighboring defect layers. The layered vacancy ordering produces isolated eight-coordinate sites.

There is thus a strong driving force to order the vacancies and the oxide and nitride anions at this composition. The resulting ordered array of coordination numbers of six, seven, and eight for the same metal is stabilized by varying the anion content of the first coordination sphere in each case. As Zr can be six or eight coordinate by oxide, it is perhaps surprising that this vacancy-ordered structure is formed rather than the pyrochlore structure, although there are no examples of monometallic pyrochlores. In the $Zr_4O_5N_2$ structure the shorter closest inter-vacancy distance ($^1/_2\langle 110\rangle_F$ compared to $^1/_2\langle 111\rangle_F$ in the pyrochlore structure) can be stabilized by the proximity of the more highly charged nitride anions. Consequently, this layered arrangement of bixbyite type vacancy patterns might therefore be expected to be unique to mixed anion systems. However, it may be involved in the bixbyite-type correlations noted recently in electron diffraction of oxide phases such as fluorite-type $Y_2Zr_2O_7$ where incommensurate C type order is observed to compete with the pyrochlore.[16] Such correlations may imply layered ordering of the type seen here.

Both the pure oxide materials Tb_2O_{3+x}[17] and the pure nitride materials U_2N_{3+x} ($0 \le x \le 1$)[18,19] adopt the

(16) Garcia-Martin, S.; Alario-Franco, M. A.; Fagg, D. P.; Feighery, A. J.; Irvine, J. T. S. *Chem. Mater.* **2000**, *12*, 1729.
(17) Baenziger, N. C.; Eick, H. A.; Schuldt, H. S.; Eyring, L. *J. Am. Chem. Soc.* **1961**, *83*, 2219.
(18) Tagawa, H.; Masaki, N. *J. Inorg. Nucl. Chem.* **1974**, *36*, 1099.

bixbyite structure at the A_2X_3 stoichiometry. The attainment of more anion-rich compositions including compositions close to A_4X_7 apparently proceeds with retention of the $Ia\bar{3}$ space group and statistical filling of up to half of the vacancies in the bixbyite structure. At compositions with $x > 0.5$ in these systems the structure type changes to an anion-defective rhombohedral modification of the fluorite structure, and there is a miscibility gap between the bixbyite type and rhombohedral type phases with apparently no compounds of precise composition A_4X_7. Comparison of these results with those for $Zr_4O_5N_2$ suggests that the new anion-vacancy ordering regime reported here is stabilized by the ordering of oxide and nitride anions.

Conclusions

Many complex superstructures of fluorite have been observed, often as unit cells in electron diffraction which have not been subsequently refined because of difficulties with crystal growth or the measurement of superstructure intensities in powder samples. $Zr_4O_5N_2$ is a well-defined and clearly refined example of a fluorite-derived superstructure not quantitatively analyzed before, although it is entirely possible that the structure type has been observed previously but not refined.

A vacancy ordering pattern stabilized by simultaneous vacancy and anion ordering produces alternate layered intergrowth of bixbyite and fluorite layers in $Zr_4O_5N_2$, which can be structurally as well as compositionally formulated as $2ZrO_2{\cdot}Zr_2ON_2$. This new A_4X_7 structure occurs rather than pyrochlore due to the ability of the nitride anions to compensate for the proximity of the anion vacancies in the bixbyite type layers. Given the extensive substitutional chemistry of the pyrochlore structure, and the wide range of coordination environments present in this layered structure, selective substitution at both the cation and anion sites appears to offer a wealth of structural chemistry in this new structure type.

Acknowledgment. We thank the EPSRC for support under GR/L60067 and for access to ISIS and the SRS. We thank Dr. R. M. Ibberson and Dr. C. C. Tang for their expert assistance on the HRPD and 2.3 diffractometers.

Supporting Information Available: PXRD patterns of γ-Zr_2ON_2 and $Zr_4O_5N_2$, and tables of bond angles (PDF). This material is available free of charge via the Internet at http://pubs.acs.org.

(19) Masaki, N.; Tagawa, H. *J. Nucl. Mater.* **1975**, *57*, 187.

CM0300415